Viscoelastic behavior of clay mineral system with liquid phase at high pressure and high temperature

Tomoya Muramoto[1,2], Yoshihiro Ito[1] and Noriyuki Furuichi[2]

[1]Research Center for Earthquake Prediction, Disaster Prevention Research Institute, Kyoto University, Uji, Kyoto, Japan

[2]National Metrology Institute of Japan (NMIJ), National Institute of Advanced Industrial Science and Technology (AIST), Tsukuba, Ibaraki, Japan

Key Points:

- Viscoelastic properties vary systematically among clay mineral species
- The viscoelastic behavior of clay mineral system with liquid phase depend on the degree of saturation
- Gradual changes from liquid-like to solid-like behavior are observed as the equilibrium shear modulus increases with increasing temperature and pressure

Abstract

We conducted dynamic viscoelastic measurements of three clay minerals in a solid–liquid two-phase state: kaolinite, illite, and smectite with water. These constituents of concentrated (dense) suspensions were investigated using a high-temperature and high-pressure rheometer, to understand tectonic and non-tectonic phenomena in the shallow part of a fault system, such as shallow slow slip events in subduction zones, and landslides on fault or bed planes. We observed shear strain rate dependencies of phase angles of both dynamic stress and strain waveforms on the rheometer at varying temperature and pressure. The pressure and temperature dependence of the viscoelastic properties of the system can be qualitatively understood by applying the Zwanzig–Mountain theory. The local packing fraction change owing to dynamic oscillations affects the changing viscoelastic properties in systems such as shallow fault systems.

Plain Language Summary

In this study, the temperature and pressure dependence of viscoelastic properties of fluid-rich kaolinite, illite, and smectite in the presence of interparticle friction was investigated as common clay mineral species on the earth surface. The viscoelastic properties can be characterized by the relationship between the stress waveform and the strain waveform. In this study, we observed oscillation strain and shear strain rate dependencies of phase angles of both dynamic stress and strain waveforms on the rheometer at varying temperature and pressure. The relationship between the grain-scale phenomena and the phenomena occurring in the shallow part of the subduction zone and landslide, as tectonic

and nontectonic phenomena, was discussed through the consideration of their phase angle behavior.

1. Introduction

Recently, various tectonic and nontectonic phenomena associated with dynamic strain such as body or surface waves of teleseism have been discovered at shallow plate boundaries and massif (e.g., Meunier et al., 2007; Wallace et al., 2012; Wallace et al., 2017; Gou et al., 2019; Miyazawa et al., 2021). This is thought to be due to the fact that dynamic strain can change the state of the ground (Van Der Elst and Brodsky, 2010). Knowledge of the response and state of the constituent materials of the crust to dynamic strain or shear response (Taylor and Brodsky, 2019) is important to improve our understanding of dynamic strain–related induced phenomena, such as shallow slow slip events (shallow SSEs), as discussed by Wallace et al. (2017), or land slide (e.g., Yamagishi and Yamazaki, 2018).

The mode of occurrence of tectonic phenomena is thought to be strongly influenced by the properties of nearby materials saturated with water, with respect to dynamic strain (Aretusini et al., 2017). Also, the properties of clay minerals under dry and wet conditions have been studied at various laboratory scales (e.g., Saffer and Marone, 2003; Kubo and Katayama, 2015). Among them, viscoelastic properties are considered to be strongly involved in the mode of occurrence of tectonic phenomena such as slow earthquakes (Goswami and Barbot, 2018). In addition, as shown by the samples collected by the International Ocean Discovery Program (IODP) (e.g., Saffer et al., 2019), a high percentage of fine-grained clay minerals are present in the shallow part of the continental crust in a water-bearing system, as shown in Saffer et al. (2019). Systematic investigation of the viscoelastic properties of these clay minerals in a solid–liquid two-phase state, especially their temperature and pressure dependence, is an important approach from a material science perspective to develop models to explain tectonic phenomena at shallow plate boundaries.

There are several examples of viscoelasticity measurements based on the assumption of tectonic phenomena (e.g., Sumita and Manga, 2008; Namiki and Tanaka, 2017). Dynamic viscoelasticity measurement based on the assumption of linear viscoelasticity (Hyun et al., 2011) is a typical measurement method, in which viscous, elastic, and viscoelastic materials are characterized using the characteristics of the phase angle between the dynamic strain waveform and the sensed stress waveform (there is also an inverse pattern of passive relationship) corresponding to the viscoelastic properties of the sample (Fig. 1). Sumita and Manga, for example, clarified the relationship between volume fraction and relaxation time using a model material. More general examples of investigating the viscoelastic properties of grains include the research on the relationship between osmotic pressure, volume fraction, and rheological parameters (G' and G'') (Evans and Lips, 1990), and the investigation of the effect of friction between solids on the rheological parameters (Shewan et al., 2021).

There are, however, no examples of dynamic viscoelasticity measurements using clay minerals as samples; accordingly, dynamic viscoelastic responses of clay minerals, such as the relaxation process (in this case, phase angle) specific to each clay mineral and their dependence on temperature and pressure are still unknown. In this study, we investigate the correspondence between dynamic strain and viscoelastic properties of clay minerals, in particular, for solid–liquid two-phase systems. We attempted to clarify the viscoelastic properties of clay minerals and their temperature and pressure dependence, by measuring representative clay minerals using a high-temperature and high-pressure rheometer. By quantitatively clarifying the viscoelastic properties of clay minerals, this study will contribute to a better understanding of the mode of occurrence of tectonic phenomena, especially the response to dynamic strain, at shallow plate boundaries.

2. Theoretical background

The purpose of this study is to clarify the temperature and pressure dependence of viscoelasticity in the case of a concentrated (dense) granular suspension system of clay minerals. In general, the viscoelasticity, friction coefficient, and stiffness of a concentrated suspension are affected by various parameters, including pressure and liquid content (Boyer et al., 2011). The shear modulus of a concentrated suspension with grain interactions can be described as follows (e.g., Zwanzig and Mountain, 1965; Evans and Lips, 1990; van der Vaart et al., 2013).

$$G_{\infty} = \rho k_B T + \left(\frac{2\pi\rho^2}{15}\right) \int_0^{\infty} g(r) \frac{d}{\mathrm{dr}} \left[r^4 \left(\frac{\mathrm{du}(r)}{\mathrm{dr}} \right) \right] dr \ldots (1)$$

where ρ is the number density of grains ($\propto$ packing fraction ϕ), k_B is Boltzmann's constant, T is absolute temperature, $g(r)$ is the pair correlation function, and $u(r)$ is the pair interaction potential. Implicit in Eq. (1), $g(r)$ and $u(r)$ express the strength of the interaction between grains in the relation with a center-to-center distance r, and here we are considering the strength of the tangential force generated when a deformable grain comes into contact with a neighboring grain. $g(r)$ is considered to have arbitrary basis functions, as shown experimentally in van der Vaart et al. (2013). Note that $\lim_{\rho \to 0} G_{\infty}(\rho) = 0$, where G_{∞} is the shear modulus of the system supported by the grain, and is commonly referred to as the equilibrium shear modulus. $u(r)$ is derived analytically and can be written as

$$u(r) = \left(\frac{32}{15}\right) d^{\frac{1}{2}} \left(d - \frac{r}{2}\right)^{\frac{5}{2}} G_P/(1-\sigma) \ldots (2)$$

where d is the diameter of the grain, G_g is the shear modulus of the grain, σ is the stress corresponding to the Poisson's ratio, and $G_P = E/[2(1+\sigma)]$. Here, E is the inherent Young ratio of the grain. In this case, because these

functions are also functions of force or pressure (Hertzian relation), Eq. (1) can be thought of as expressing the equilibrium shear modulus of the entire system, which depends on temperature, pressure, and density. In order to express the effect of pressure explicitly, we can consider the relationship between the bulk modulus (K_∞) and Eq. (1). The relationships among pressure, equilibrium shear modulus, and bulk modulus are not linearly independent as follows:

$$K_\infty = \frac{5}{8} G_\infty + 2(P - \rho k_B T) \ldots (3)$$

Next, we consider the relationship between the equilibrium shear modulus and the phase angle (e.g., Berker, 2002). The relationship between the stress waveform $\sigma_w(t)$, strain waveform $\gamma(t)$, and equilibrium shear modulus can be described as follows:

$$\frac{\sigma_w(t_\delta)}{\gamma_c} = \varphi(t_\delta) + G_\infty \ldots (4)$$

$\frac{\sigma_w(t_\delta)}{\gamma_c}$ corresponds to the relaxation modulus, which can be decomposed into the relaxation function $\varphi(t_\delta)$ and G_∞, which behaves viscously. γ_c is the applied constant strain. Here, the equilibrium shear modulus corresponds to the static behavior; when $\varphi(t_\delta) \neq 0$, Eq. (4) gives the relaxation modulus of an elastic body with a relaxation time (t_δ). In dynamic viscoelasticity measurements, the strain is sinusoidal and can be described as follows:

$$\gamma(t) = \gamma_0 e^{\mathrm{i}\, t} \ldots (5)$$

where γ_0 is the maximum amplitude of the strain waveform (oscillation strain), ω is the oscillation frequency. Following Eqs. (4) and (5), $\sigma_w(t)$, which has a sinusoidal component that behaves viscously and a sinusoidal component that behaves "solid-like" in dynamic viscoelasticity measurements, can be naturally defined as follows:

$$\sigma_w(t) \equiv G_\infty \gamma(t) + \sigma_0 e^{i(\omega t + \delta)} \ldots (6)$$

Here, σ_0 is the maximum stress of the sensed stress waveform. The first term on the right-hand side is the component with solid-like behavior that has no phase angle, and the second term on the right-hand side is the component with viscous behavior that has a phase angle, which is a specific description of the relaxation function. Eqs. (5) and (6) and the complex modulus G^*, the relationship between the measurement principle of dynamic viscoelasticity and equilibrium shear modulus can be clearly described as follows:

$$G^* = \frac{\sigma_w(t)}{\gamma(t)} = G_\infty + \left(\frac{\sigma_0}{\gamma_0}\right) e^{\mathrm{i}} \equiv (G_\infty + G') + iG'' \ldots (7)$$

$$G' = \left(\frac{\sigma_0}{\gamma_0}\right) cos\delta \ldots (8)$$

$$G'' = \left(\frac{\sigma_0}{\gamma_0}\right) sin\delta \ldots (9)$$

where G' is the storage modulus, G'' is the loss modulus. In addition, the relationship between the effect of pressure compaction and viscoelasticity can also be captured by considering it via packing fraction, which is described in detail in Mason et al. (1995). The packing fraction is also a function of velocity (Srivastava et al., 2021), and can be written in the form of a power law as follows:

$$\phi = \phi^0 - a * I^{a_2} \ldots (10)$$

where ϕ^0 is the initial packing fraction and I (inertial number) is defined as the dimensionless shear rate as follows.

$$I = \frac{\dot{\gamma} d}{\sqrt{P/\rho_g}} \ldots (11)$$

where $\dot{\gamma}$ is the shear strain rate and ρ_g is the mass density of the grain. Given that ρ is the number density, and $\rho \equiv N/V$ using system volume V and number of grains in system N, the packing fraction is related to ρ as follows:

$$\rho \propto \phi N \ldots (12)$$

$$\phi = V_g/V \ldots (13)$$

where V_g is the total volume of grains in the system. In addition, there is an empirical relationship between the total volume of grains and pressure as follows (e.g., Panelli and Filho, 2001):

$$V_g = 1/(b * \ln P + b_2) \ldots (14)$$

3. Experimental methodology

We used our own high-temperature and high-pressure rheometer assembly for the measurements (Fig. 2). The rheometer used in this study is based on and modified from a coaxial cylindrical rheometer (e.g., Webb et al., 2012). Liquid pressurization is used to raise the pressure to avoid gas mixing with the sample under high-pressure conditions, which would change the properties of the sample (Koran and Dealy, 1999). We specified the oscillation frequency and maximum

oscillation amplitude of the rotor, and measured the shear stress. The angular frequency was set to 0.02 Hz. (This frequency is equivalent to the dominant frequency of very low frequency earthquakes (e.g., Baba et al., 2020).) We used a rotor with a cone angle of 15° and $R = 13$ mm, and a high-pressure vessel holding the sample with $L = 14$ mm. The rotor was made of stainless steel (SUS) with a smooth surface, and preliminary experiments confirmed that there was no significant slip on the contact surface with the sample. Pressurization was carried out using a pressurized pump with water as the medium. A Peltier jacket and constant temperature bath were used to control the temperature and provide sufficient soak time.

The following steps were taken to set up the sample as shown in Fig. 2 and conduct the experiment: Step 1, a solid (clay mineral) sample was prepared with water added to adjust the wt% of the solid; Step 2, the sample was placed in a high-pressure vessel; Step 3, a rotor was inserted; Step 4, oil was injected (pressure transfer medium: dioctyl sebacate (e.g., Muramoto et al., 2020)) into the vessel; Step 5, the apparatus was repeatedly pressurized and depressurized to release air; Step 6, the apparatus was pressurized and maintained at a constant pressure; Step 7, a constant normal stress was maintained on the rotor; and Step 8, the temperature was set, and then the experiment was conducted. Because the applied pressure (confining pressure) was sufficiently large compared to the swelling pressure (e.g., Stucki et al., 2000), no significant noise due to the edge effect was observed. Step 4 is a procedure to prevent the wt% adjusted in Step 1 from changing during the experiment. The normal stress set by the procedure in Step 7 was successfully controlled with a deviation of <1%. In this study, two main types of experiments were conducted. The first was an experiment in which we swept the oscillation strain from 0 to 10%. The other was an experiment in which the temperature was swept from 30 to 120°C. For kaolinite (NaRiKa Corporation) and illite (Grüne Tonerde, Argiletz Laboratories), which were used as samples, experiments were conducted with a wt% of 62.5%. For smectite (Hayashi Pure Chemical Ind., Ltd.), experiments were conducted with three wt% values: 15%, 20%, and 25%. Note that smectite has a higher water-holding capacity than the other two clay minerals (e.g., Salles et al., 2010), so the setting of the wt% value differed from the others.

4. Results

The results of the measurements of kaolinite and illite with fluid pressures of 3.45 MPa and 10.34 MPa showed that the phase angle was between 0 and 4° within a range of 10% oscillation strain (Fig. 3). It can be seen that the phase angle of both kaolinite and illite tended to be lower at higher pressures. In both cases, as the oscillation strain increased, the phase angle tended to increase. It is important to note that because we used a constant angular frequency for our measurements, the oscillation strain (amplitude) is a function of shear strain rate. In the case of kaolinite, the behavior was exponential, and in the case of illite, the behavior was such that the phase angle hit its limit at around 2°. In the case of low pressure for illite, a sharp increase in the phase angle was

observed when the oscillation strain was between 1% and 3%.

For smectite, we compared the experimental results for three values of wt% from 15% to 25% (Fig. 4). In the case of low pressure, the smaller the wt%, the larger the phase angle tended to be. In the results for the same samples under higher pressure, there was no significant difference between the samples with different wt%. The overall trend (Figs. 3 and 4) was that the larger the oscillation strain (or shear strain rate), the larger the phase angle tended to be. This means that the larger the oscillation strain (or shear strain rate), the softer, or more liquid-like the sample tends to be from hard, or solid-like state. Although the wt% of smectite was smaller than that of kaolinite and illite, the phase angle of smectite tended to be smaller than that of kaolinite and illite, indicating that the sample was solid-like against dynamic strain.

The phase angle of kaolinite and illite tended to decrease as the temperature increased (Fig. 5). In contrast, in the case of smectite, there were discontinuities in the measured values between 20 and 25 wt%, and there was an inflection point around 60°C (Fig. 6).

To better discuss the results of the experiments, we performed model calculations (Fig. 7) using Eqs. (3) and (10)–(14). In this calculation, the bulk modulus was assumed to be constant. The shear strain rates were representative values (maximum velocity in every oscillation step) in the middle point of rotor. Although the results vary greatly depending on the model parameters, it was found that under the conditions shown in Fig. 7, the equilibrium shear modulus varied ~20% within a range of ~10% of oscillation strain. The equilibrium shear modulus tended to increase with increasing pressure, the equilibrium shear modulus tended to increase with increasing temperature, and the equilibrium shear modulus tended to decrease with swelling. These three points were more pronounced at lower pressures.

5. Discussion

The result of this study, in which the phase angle decreased with increasing temperature and pressure, is quite natural (Eqs. (1)–(14)). In terms of the friction coefficient (or stiffness), it is known that the friction coefficient of various clay minerals increases with temperature (e.g., Kubo and Katayama, 2015), and empirical models such as the rate and state law (e.g., Ruina, 1983) also include the effect of temperature (e.g., Frost and Ashby, 1982; Ruina, 1983). Although the temperature dependence of clay minerals has been well studied in friction experiments, this is the first time that the temperature and pressure dependence of viscoelasticity of clay minerals has been revealed. Because the wt% was set low and the fraction of liquid phase was very high in the case of using smectite, the effect of the decrease in viscosity of the liquid phase with the increase of temperature may be seen in the results. In other words, the tendency for the phase angle to increase at temperatures up to 60°C may be attributed to the decrease in the viscosity of the liquid phase. In addition, although kaolinite and illite displayed a similar downward trend, the trend changed at 80°C and

100°C for the 25% and 20% wt% cases. This may be due to the change in the local packing fraction caused by the dehydration reaction associated with the process of metamorphosis of smectite into illite (I/S metamorphism) (e.g., Du et al., 2021). The time taken for the measurement (soak time) was almost same for the three patterns, and the trend change occurred earlier for larger wt%, which strongly suggests that local dehydration occurred. Experiments with a wider range of temperature and pressure measurements may allow for better comparison with previous studies of I/S metamorphism. This is a subject for future work.

Wt% can be roughly read as volume fraction, and trend of our results is similar to that of previous studies obtained with concentrated spherical suspensions (e.g., Shikata and Pearson, 1994). The results of the measurements with varying wt% (Fig. 4 left) support the statement of Mason et al. (1995) and are in accordance with Eqs. (1)–(3) (Zwanzig–Mountain theory) assuming that the density decreases with local swelling (Eqs. (10)–(12)). The results measured at 10.34 MPa were independent of wt%, suggesting that the effective packing fraction may be saturated due to the large confining pressure (Deike et al., 2001). The phenomenon of the phase angle increasing as the oscillation strain or shear strain rate increases is in accordance with the change in the effective packing fraction (Eq. (10)) and is also consistent with the framework of Mason et al (1995) and Zwanzig–Mountain theory.

Next, we discuss the measurements obtained in this study in comparison with the results of model calculations (Fig. 7) performed using Eqs. (3) and (10)–(14). The results of the calculations support the measurements obtained in this study. The equilibrium shear modulus tends to increase with increasing pressure, the equilibrium shear modulus tends to increase with increasing temperature, and the equilibrium shear modulus tends to decrease with swelling. These three points, which are more pronounced at lower pressures, are considered complementary to the measurement results obtained in this study. Although the complex modulus in this study cannot be calculated from the measurements (note that it is different from the general complex modulus), the equilibrium shear modulus and G' in the form of Eq. (7) can be expressed as a solid-like part, which suggests that the equilibrium shear modulus is a parameter that cannot be ignored in dynamic viscoelasticity measurements. This suggests that it is valid to discuss the measurement along the theoretical background we described.

The temperature and pressure conditions implemented in this study correspond to the shallow (~10 km) temperature and pressure conditions in the subduction zone. In the case of shallow SSEs, which are representative of phenomena occurring in such regions, it has been suggested that there are mechanical processes involving fluid movement in the region where they occur (Warren-Smith et al., 2019). The results of the present study may provide support for such a previous study. For example, the results of the present study, in which the elastic weakens (the phase angle increases) as the shear strain rate increases, can be re-

garded as a kind of weakening, which may be complementary to previous studies on the mechanism of the relationship between velocity weakening and shallow SSEs. In other words, systematic investigation of viscoelasticity of materials in the form of the present study may be useful for the development of dynamical modeling of SSEs or landslides with spatial contrast of viscoelasticity. Although the wt% of smectite was smaller than that of kaolinite and illite, the phase angle of smectite tended to be smaller than that of kaolinite and illite, indicating that the sample was in a "stable" state against dynamic strain (Figs. 3 and 4). This implies that the initial process of landslide triggered by earthquakes is material dependent. For example, this study suggests that there is a material dependence in the empirical models that relate the likelihood of landslide occurrence to PGA (peak ground acceleration) and PGV (peak ground velocity). In other cases, when considering the elastic weakening process (e.g., Jia et al., 2011) due to dynamic strain in the shallow part of the subduction zone, the contribution of elastic weakening of kaolinite and illite is considered to be larger than that of smectite (under low temperature conditions). Under high-temperature conditions, I/S metamorphism progresses and the proportion of kaolinite and illite increases compared to that of smectite, suggesting that kaolinite is more dominant in the elastic weakening process under high-temperature conditions more severe than in Fig. 6. In addition, the knowledge of viscoelasticity depending on the initial saturation (wt%) may be very important to consider the diffusion process of fluid in the ground.

6. Conclusions

In this study, dynamic viscoelasticity measurements were carried out on three clay minerals, kaolinite, illite, and smectite, using a custom-designed high-temperature and high-pressure rheometer assembly, in order to clarify the temperature and pressure dependence of their viscoelastic properties. As a result, it was found that the phase angle depends on the amplitude of the oscillation strain or the shear strain rate. The viscoelastic properties of the clay minerals differ systematically among the minerals tested, and their temperature and pressure dependence can be qualitatively explained by the Zwanzig–Mountain theory. The differences between minerals may be due to differences in microscopic mechanisms, such as atomic-scale thermally active processes, which cannot be discussed deeply from macroscopic measurements as in this study. Although the temperature and pressure conditions implemented in this study are very limited, we expect to obtain results that can be used for more useful discussion when we conduct experiments under a wider range of conditions. Further measurements over a wider temperature and pressure range will be necessary to provide a complete picture with appropriate modeling using appropriate approximations. We hope that this study will be a very useful starting point for understanding the viscoelastic processes in the earth science phenomena.

Acknowledgments

This work was supported by JSPS KAKENHI Grant No. JP19K15494.

Data Availability Statement

Correspondence and requests for additional material should be addressed to muramoto.tomoya@aist.go.jp. All experimental raw data used in figures in this manuscript are available in Zenodo with the identifier (10.5281/zenodo.6360823). The rights for the code used in the calculations in Fig. 7 belong to the authors. If you wish to use the code, please contact to muramoto.tomoya@aist.go.jp with the reason for use.

References

Aretusini, S., Mittempergher, S., Plümper, O., Spagnuolo, E., Gualtieri, A. F., & Di Toro, G. (2017). Production of nanoparticles during experimental deformation of smectite and implications for seismic slip. *Earth and Planetary Science Letters*, *463*, 221–231. https://doi.org/10.1016/j.epsl.2017.01.048

Baba, S., Takeo, A., Obara, K., Matsuzawa, T., & Maeda, T. (2020). Comprehensive detection of very low frequency earthquakes off the Hokkaido and Tohoku pacific coasts, Northeastern Japan. *Journal of Geophysical Research: Solid Earth*, *125*(1), 1–13. https://doi.org/10.1029/2019JB017988

Berker, A. (2002). Rheology for adhesion science and technology. *Adhesion Science and Engineering*, *12*, 443–498. https://doi.org/10.1016/B978-0-444-51140-9.50039-1

Boyer, F., Guazzelli, É., & Pouliquen, O. (2011). Unifying suspension and granular rheology. *Physical Review Letters*, *107*(18), 188301. https://doi.org/10.1103/PhysRevLett.107.188301

Deike, I., Ballauff, M., Willenbacher, N., & Weiss, A. (2001). Rheology of thermosensitive latex particles including the high-frequency limit. *Journal of Rheology*, *45*(3), 709–720. https://doi.org/10.1122/1.1357820

Du, J., Cai, J., Chao, Q., Song, M., & Wang, X. (2021). Variations and geological significance of solid acidity during smectite illitization. *Applied Clay Science*, *204*. https://doi.org/10.1016/j.clay.2021.106035

Evans, I. D., & Lips, A. (1990). Concentration dependence of the linear elastic behaviour of model microgel dispersions. *Journal of the Chemical Society, Faraday Transactions*, *86*(20), 3413–3417. https://doi.org/10.1039/FT9908603413

Frost, H. J., & Ashby, M. F. (1982). Deformation-Mechanism Maps, Pergamon, New York, 166

Goswami, A., & Barbot, S. (2018). Slow-slip events in semi-brittle serpentinite fault zones. *Scientific Reports*, *8*(1), 6181. https://doi.org/10.1038/s41598-018-24637-z

Gou, T., Huang, Z., Zhao, D., & Wang, L. (2019). Structural heterogeneity and anisotropy in the source zone of the 2018 eastern Iburi earthquake in Hokkaido, Japan. *Journal of Geophysical Research: Solid Earth*, *124*(7), 7052–7066. https://doi.org/10.1029/2019JB017388

Hyun, K., Wilhelm, M., Klein, C. O., Cho, K. S., Nam, J. G., Ahn, K. H., … McKinley, G. H. (2011). A review of nonlinear oscillatory shear tests: Analysis and application of large amplitude oscillatory shear (LAOS). *Progress in Polymer Science*, *36*(12), 1697–1753. https://doi.org/10.1016/j.progpolymsci.2011.02.002

Jia, X., Brunet, T., & Laurent, J. (2011). Elastic weakening of a dense granular pack by acoustic fluidization: Slipping, compaction, and aging. *Physical Review. E, Statistical, Nonlinear, and Soft Matter Physics*, *84*(2 Pt 1), 020301. https://doi.org/10.1103/PhysRevE.84.020301

Koran, F., & Dealy, J. M. (1999). A high pressure sliding plate rheometer for polymer melts. *Journal of Rheology*, *43*(5), 1279–1290. https://doi.org/10.1122/1.551046

Kubo, T., & Katayama, I. (2015). Effect of temperature on the frictional behavior of smectite and illite. *Journal of Mineralogical and Petrological Sciences*, *110*(6), 293–299. https://doi.org/10.2465/jmps.150421

Mason, T. G., Bibette, J., & Weitz, D. A. (1995). Elasticity of compressed emulsions. *Physical Review Letters*, *75*(10), 2051–2054. https://doi.org/10.1103/PhysRevLett.75.2051

Meunier, P., Hovius, N., & Haines, A. J. (2007). Regional patterns of earthquake triggered landslides and the

Miyazawa, M., Brodsky, E. E., & Guo, H. (2021). Dynamic earthquake triggering in Southern California in high resolution: Intensity, time decay, and regional variability. *AGU Advances*, *2*(2), 1–15. https://doi.org/10.1029/2020AV000309

Muramoto, T., Kajikawa, H., Iizumi, H., & Ide, K., & Fujita, Y. (2020). Design of a high-pressure viscosity-measurement system using two pressure balances. *Measurement Science and Technology, 31*(11) 115302. https://iopscience.iop.org/article/10.1088/1361-6501/ab9cd

Namiki, A., & Tanaka, Y. (2017). Oscillatory rheology measurements of particle- and bubble-bearing fluids: Solid-like behavior of a crystal-rich basaltic magma. *Geophysical Research Letters*, *44*(17), 8804–8813. https://doi.org/10.1002/2017GL074845

Panelli, R., & Ambrozio Filho, F. (2001). A study of a new phenomenological compacting equation. *Powder Technology*, *114*(1–3), 255–261. https://doi.org/10.1016/S0032-5910(00)00207-2

Ruina, A. (1983). Slip instability and state variable friction laws. *Journal of Geophysical Research: Solid Earth, 88*(B12), 10359–10370. https://doi.org/10.1029/JB088iB12p10359

Saffer, D. M., & Marone, C. (2003). Comparison of smectite- and illite-rich gouge frictional properties: Application to the updip limit of the seismogenic zone along subduction megathrusts. *Earth and Planetary Science Letters*, *215*(1–2), 219–235. https://doi.org/10.1016/S0012-821X(03)00424-2

Saffer, D. M., Wallace, L. M., Barnes, P. M., Pecher, I. A., Petronotis, K. E., LeVay, L. J., … Wu, H. -Y. (2019). Expedition 372B/375 summary. *Proceedings of the International Ocean Discovery Program*, *372b*(375). https://doi.org/10.14379/iodp.proc.372B375.101.2019

Salles, F., Bildstein, O., Douillard, J. M., Jullien, M., Raynal, J., & Van Damme, H. (2010). On the cation dependence of interlamellar and interparticular water and swelling in smectite clays. *Langmuir*, *26*(7), 5028–5037. https://doi.org/10.1021/la1002868

Shewan, H. M., Yakubov, G. E., Bonilla, M. R., & Stokes, J. R. (2021). Viscoelasticity of non-colloidal hydrogel particle suspensions at the liquid–solid transition. *Soft Matter*, *17*(19), 5073–5083. https://doi.org/10.1039/d0sm01624a

Shikata, T., & Pearson, D. S. (1994). Viscoelastic behavior of concentrated spherical suspensions. *Journal of Rheology*, *38*(3), 601–616. https://doi.org/10.1122/1.550477

Srivastava, I., Silbert, L. E., Grest, G. S., & Lechman, J. B. (2021). Viscometric flow of dense granular materials under controlled pressure and shear stress. *Journal of Fluid Mechanics*, *907*, (A18) https://doi.org/10.1017/jfm.2020.811

Stucki, J. W., Wu, J., Gan, H., Komadel, P., & Banin, A. (2000). Effects of iron oxidation state and organic cations on dioctahedral smectite hydration. *Clays and Clay Minerals*, *48*(2), 290–298. https://doi.org/10.1346/CCMN.2000.0480216

Sumita, I., & Manga, M. (2008). Suspension rheology under oscillatory shear and its geophysical implications. *Earth and Planetary Science Letters*, *269*(3–4), 468–477. https://doi.org/10.1016/j.epsl.2008.02.043

Taylor, S. E., & Brodsky, E. E. (2019). Energy Partitioning in Granular Flow Depends on Mineralogy via Nanoscale Plastic Work. *Journal of Geophysical Research: Solid Earth*, *124*(7), 6397–6408. https://doi.org/10.1029/2019JB017762

Van Der Elst, N. J., & Brodsky, E. E. (2010). Connecting near-field and far-field earthquake triggering to dynamic strain. *Journal of Geophysical Research*, *115*(B7), 1–21. https://doi.org/10.1029/2009JB006681

van der Vaart, K., Rahmani, Y., Zargar, R., Hu, Z., Bonn, D., & Schall, P. (2013). Rheology of concentrated soft and hard-sphere suspensions. *Journal of Rheology*, *57*(4), 1195–1209. https://doi.org/10.1122/1.4808054

Wallace, L. M., Beavan, J., Bannister, S., & Williams, C. (2012). Simultaneous long-term and short-term slow slip events at the Hikurangi subduction margin, New Zealand: Implications for processes that control slow slip event occurrence, duration, and migration. *Journal of Geophysical Research: Solid Earth*, *117*(B11), n/a–n/a. https://doi.org/10.1029/2012JB009489

Wallace, L. M., Kaneko, Y., Hreinsdóttir, S., Hamling, I., Peng, Z., Bartlow, N.,

D'Anastasio, E., & Fry, B. (2017). Large-scale dynamic triggering of shallow slow slip enhanced by overlying sedimentary wedge. *Nature Geoscience*, *10*(10), 765–770. https://doi.org/10.1038/ngeo3021

Warren-Smith, E., Fry, B., Wallace, L., Chon, E., Henrys, S., Sheehan, A., … Lebedev, S. (2019). Episodic stress and fluid pressure cycling in subducting oceanic crust during slow slip. *Nature Geoscience*, *12*(6), 475–481. https://doi.org/10.1038/s41561-019-0367-x

Webb, E. B., Rensing, P. J., Koh, C. A., Sloan, E. D., Sum, A. K., & Liberatore, M. W. (2012). High pressure rheometer for in situ formation and characterization of methane hydrates. *Review of Scientific Instruments*, *83*(1), 015106. https://doi.org/10.1063/1.3675889

Yamagishi, H., & Yamazaki, F. (2018). Landslides by the 2018 Hokkaido Iburi-Tobu earthquake on September 6. *Landslides*, *15*(12), 2521–2524. https://doi.org/10.1007/s10346-018-1092-z

Zwanzig, R., & Mountain, R. D. (1965). High-frequency elastic moduli of simple fluids. *The Journal of Chemical Physics*, *43*(12), 4464–4471. https://doi.org/10.1063/1.1696718

Figure captions:

Figure 1.

1. Stress and strain profiles of elastic, viscoelastic, and viscous materials.
2. Various materials characterized by strain and stress waveforms: diagrams of a simple lattice model and graphs of measured values (: phase angle)

Figure 2.

Experimental system configuration

Figure 3.

Phase angle as a function of oscillation strain and shear strain rate for kaolinite (wt% = 62.5%), illite (wt% = 62.5%) and smectite (wt% = 15%) measured at 3.45 MPa (orange) and 10.34 MPa (green)

Figure 4.

Phase angle as a function of oscillation strain and shear strain rate for smectite with different wt% at 3.45 MPa (orange) and 10.34 MPa (green)

Figure 5.

Phase angle as a function of temperature for kaolinite and illite (wt% = 62.5%)

Figure 6.

Phase angle as a function of temperature for smectite with different wt%

Figure 7.

Equilibrium shear modulus as a function of oscillation strain and shear strain rate for comparison with different pressure and temperature as the result of model calculation using Eqs. (3), (10) – (14). $\rho_g = 2650\ kg/m^3$, $d = 4$ m, $K_\infty = 5.0 * 10^9$ Pa, $a = 2.0 * 10^8$, $a_2 = 1.04$, $b = 1.0 * 10^4$ and $b_2 = 8.0 * 10^6$ were used as the parameters in the model calculation. N was treated as a parameter that can take on arbitrary values, and we set $N * k_B \cong 1$.

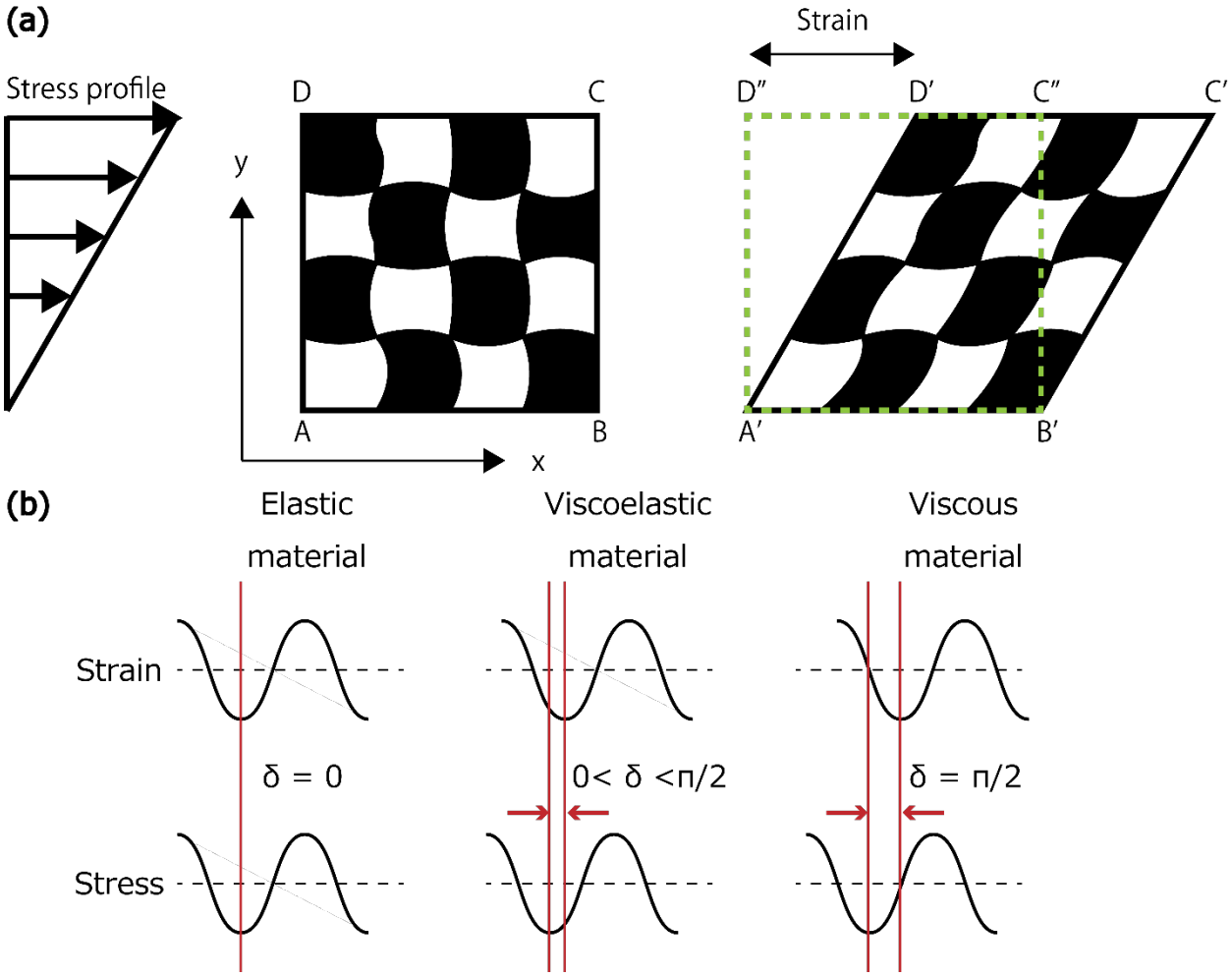

Fig. 1

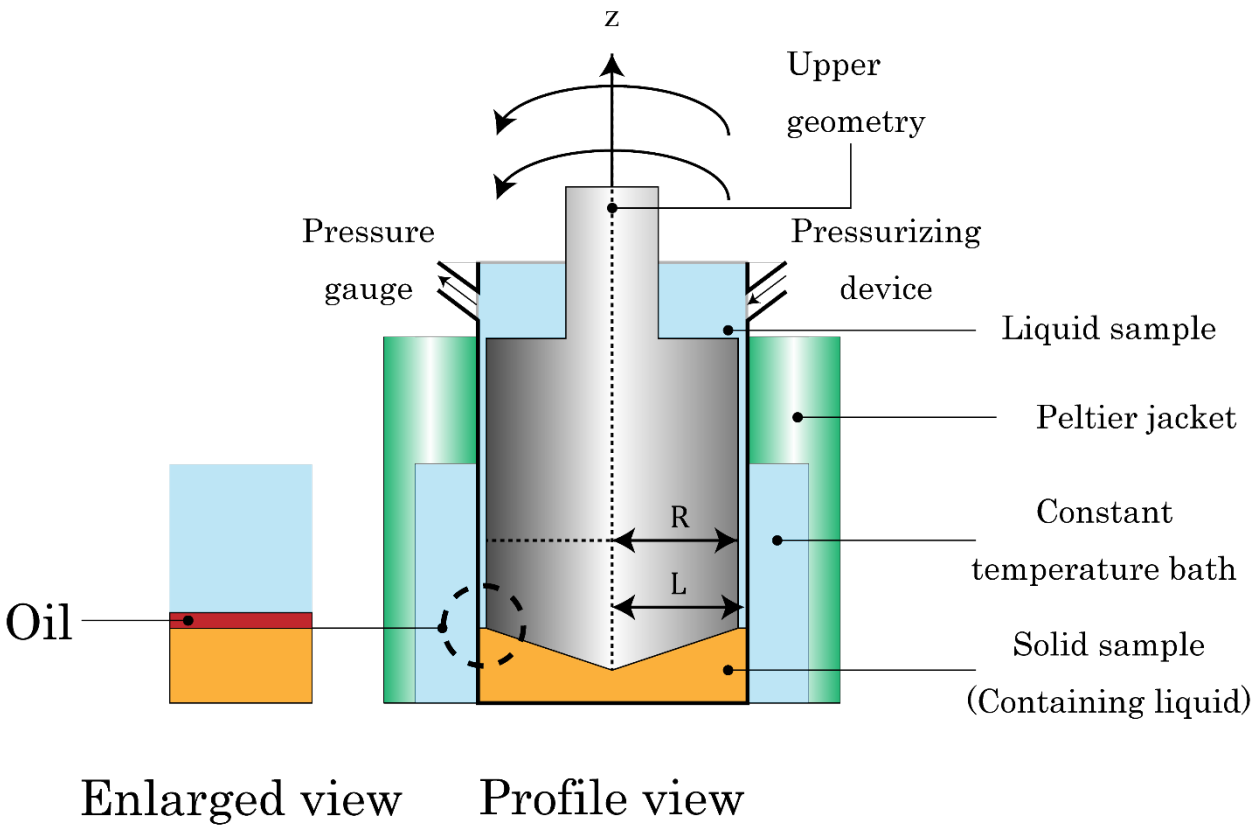
z
Upper
geometry
Pressure
gauge
Pressurizing
device
Liquid sample
Peltier jacket
Constant
temperature bath
R
L
Oil
Solid sample
(Containing liquid)
Enlarged view
Profile view

Fig. 2

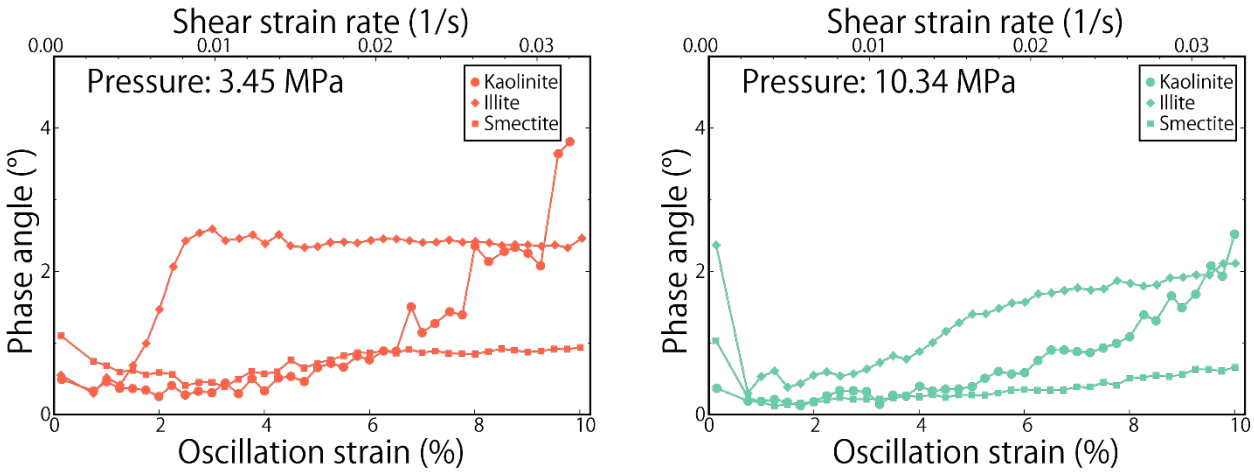
Shear strain rate (1/s)
0.00
0.01
0.02
0.03
Pressure: 3.45 MPa
Kaolinite
Illite
Smectite
Phase angle (°)
Oscillation strain (%)
Shear strain rate (1/s)
Pressure: 10.34 MPa
Kaolinite
Illite
Smectite
Phase angle (°)
Oscillation strain (%)

Fig. 3

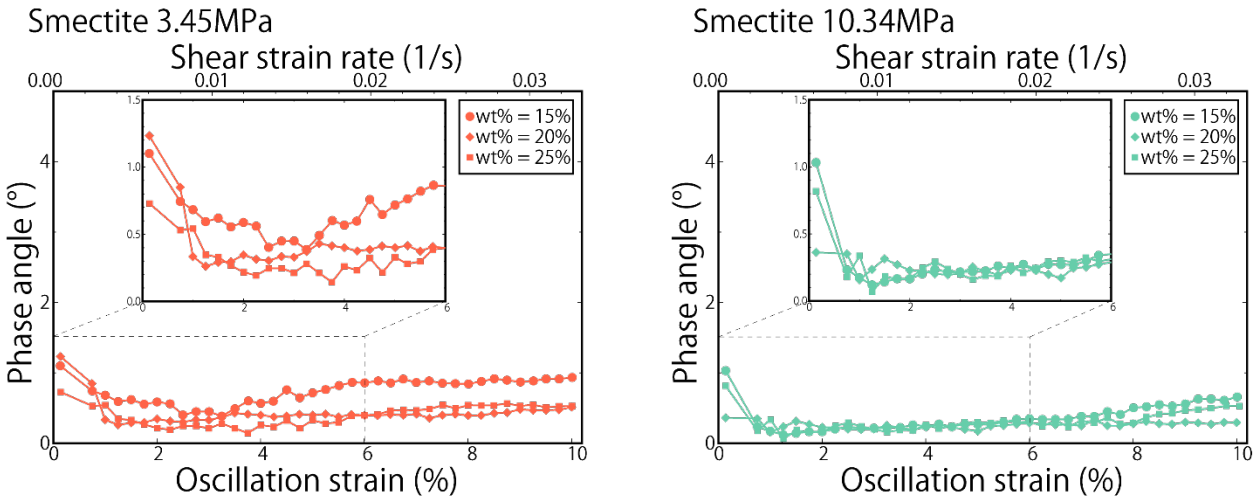
Smectite 3.45MPa
Shear strain rate (1/s)
0.00
0.01
0.02
0.03
wt% = 15%
wt% = 20%
wt% = 25%
Phase angle (°)
Oscillation strain (%)
Smectite 10.34MPa
Shear strain rate (1/s)
0.00
0.01
0.02
0.03
wt% = 15%
wt% = 20%
wt% = 25%
Phase angle (°)
Oscillation strain (%)

Fig. 4

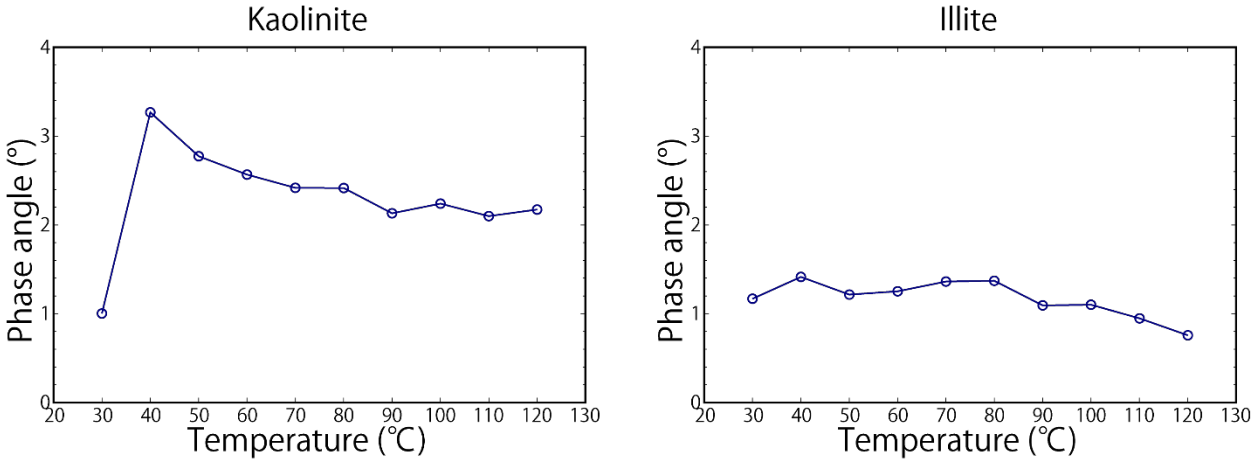
Kaolinite
Phase angle (°)
Temperature (℃)
Illite
Phase angle (°)
Temperature (℃)

Fig. 5

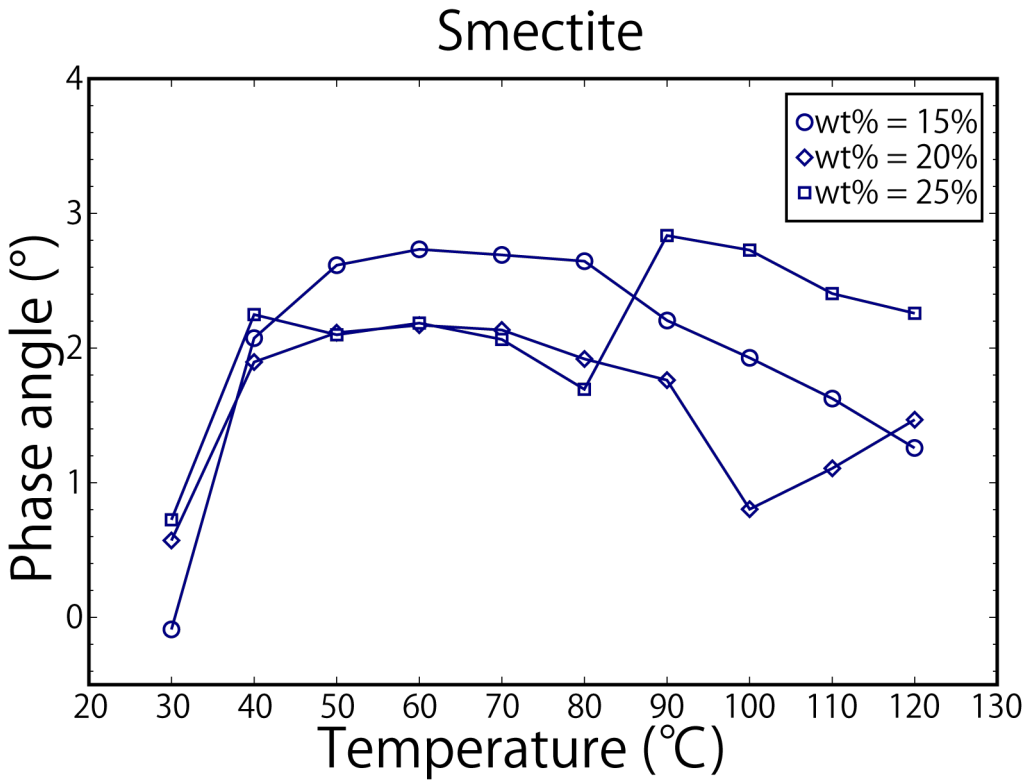
Smectite
wt% = 15%
wt% = 20%
wt% = 25%
Phase angle (°)
Temperature (°C)
0
1
2
3
4
20
30
40
50
60
70
80
90
100
110
120
130

Fig. 6

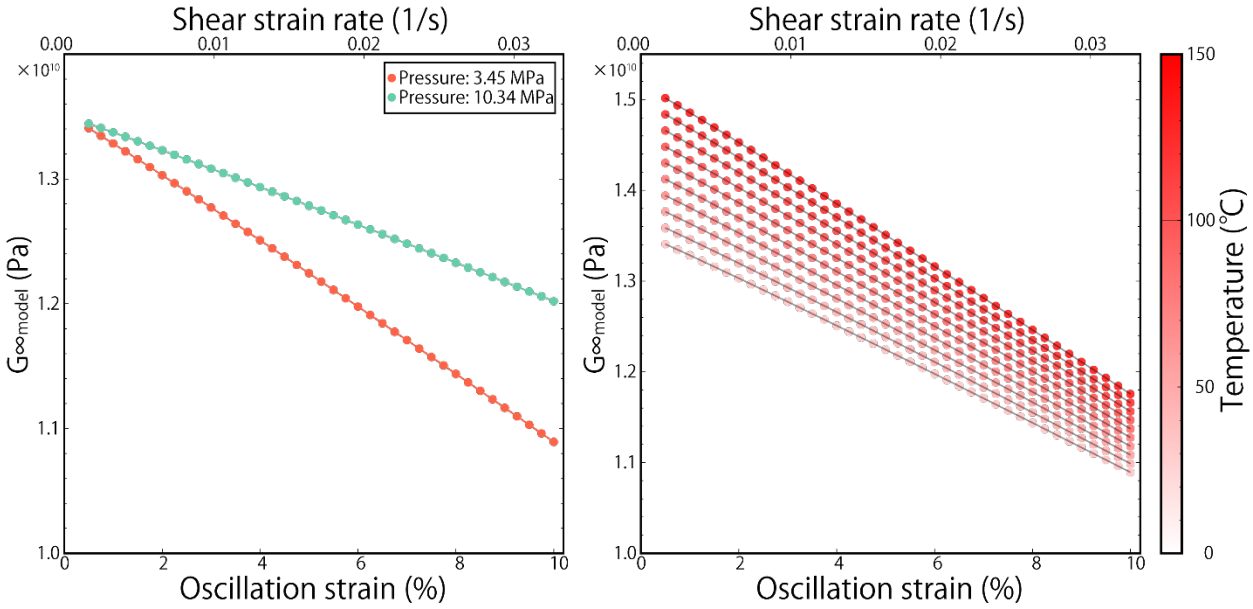
Shear strain rate (1/s)
Pressure: 3.45 MPa
Pressure: 10.34 MPa
G∞model (Pa)
Oscillation strain (%)
Temperature (°C)

Fig. 7